



Strain capacity of cross-section elements and the role of local slenderness in the rotation capacity of structural steel

S. Torabian¹, B.W. Schafer²

Abstract

The objective of this paper is to demonstrate how element (e.g. flange) local slenderness may be used to predict element strain capacity, and in turn, the element strain capacity may be used to predict member rotational capacity in structural steel members. Member plastic hinge rotation capacity has an important role in the design of steel structures, and while implicit understanding of the rotation capacity has sufficed in the past, as inelastic direct analysis methods are adopted in conventional as well as seismic design more explicit treatments are needed. It is hypothesized that the member rotation capacity, for rotations limited by local buckling, may be determined based on comparing the strain demands based on the distance to the neutral axis, against the strain capacity determined as a function of the element local slenderness. To test this hypothesis a comprehensive series of material and geometric shell finite element collapse analysis are performed in ABAQUS on component elements (plates) and structural steel members. The finite element analysis confirms the hypothesis, and also demonstrates the importance of additional factors, such as depth-to-length (shear-to-moment) in predicting the rotational capacity. The analyses are compared to existing code provisions for both conventional and seismic design and recommendations for potential improvements are made.

1. Introduction

In design of hot-rolled (structural) steel structures, classification of structural members for local buckling is a common approach in most current design codes such as AISC (2010a) and Eurocode 3 (EC3 2005). Classifications are generally considered to connect member strength or ductility capacity to element characteristics such as width-to-thickness ratio and boundary conditions (stiffened or unstiffened elements). Both of these element characteristics can be interpreted as member local slenderness by considering proper plate buckling coefficients (Seif and Schafer 2010). In Chapter B of the AISC specification, sections are classified as containing compact, noncompact, and/or slender elements (AISC 2010a). For each classification, a different design method or provision is presented to account for element slenderness in determination of

¹ School of Civil Engineering, College of Engineering, University of Tehran, <torabian@ut.ac.ir>
Visiting Researcher, Department of Civil Engineering, Johns Hopkins University, <storabi2@jhu.edu>

² Professor and Chair, Department of Civil Engineering, Johns Hopkins University, <schafer@jhu.edu>

the member strength. These classifications are considered for members subjected to axial compression, flexure, or combined flexure and axial compression (i.e., beam-columns).

On the other hand, another section classification scheme is set forth in the AISC Seismic Provisions (AISC 2010b) which addresses the ductility capacity of the section in terms of axial or rotational ductility. In this classification, the sections are classified as “highly ductile” or “moderately ductile” members. Seismic Force Resisting Systems (SFERS) determine the ductility demands of the members considered to provide ductility for the system. Generally, a more ductile SFERS would impose more ductility demands on the members and therefore members should fulfill the requirement of “highly ductile” members.

Appendix 1 of the AISC specification (AISC 2010a) lets designers use inelastic methods in analysis and design of non-seismic controlled structures. As a requirement for the use of the inelastic analysis methods, the structural members must have a certain amount of ductility at the point of plastic hinges. Although ductility demands at the plastic hinges could be determined precisely by means of plastic analyses, instead the code requires the engineer to provide a minimum required rotation capacity ($R_{cap}=3$) for the section, where R_{cap} is a dimensionless parameter used to show the rotation ductility of the section (see Section 4). This is established by using “compact” cross-sectional elements along with some additional modifications, and providing more closely spaced lateral bracing. Thus, the relation between cross-sectional or member characteristics and the ductility capacity is not explicitly discussed.

In seismic analysis, or the design and rehabilitation of structures, determination of the member ductility as a function of the cross-section characteristics is essential. This information is needed for both modeling parameters and acceptance criteria, as discussed in FEMA-356 (FEMA 2000) and ASCE-41-06 (ASCE 2007). Currently, both the modeling parameters and acceptance criteria for plastic deformations are connected to either beam flange width-to-thickness or web depth-to-thickness ratios and a linear interpolation is adopted for values in-between.

Almost all current design codes consider a step-wise approach in classification of sections that may result in nonoptimal design of steel members for both strength and ductility demands. While an inherent continuous change in structural capacity in terms of strength or ductility is anticipated by changing the member slenderness, design codes provide essentially lower-bound solutions over specific classification regimes, and ignore the reserve capacities between the classification limits. As a general motivation, improving current code-based approaches and making cross-section and member characteristics more explicit in the determination of member capacity (strength or ductility) would be potentially beneficial and could culminate in more realistic and optimized steel structures.

Another related issue on the local buckling limits of the current code is that the interaction between the elements, such as flanges and web, are not considered explicitly in all cases. A detailed study on element interaction showed that the code limitations could be modified to consider the interaction between the section elements more precisely (Seif and Schafer 2010).

In recent years, a new deformation-based design approach termed the Continuous Strength Method (CSM) has been proposed to determine the resistance of compact and non-compact

stainless steel structural members based on the deformation capacity of cross-section elements. Recently, CSM has been extended to other materials and various cross-sections composed of flat plates (Gardner and Nethercot 2004a, Ashraf et al. 2006a, Ashraf et al. 2008). CSM does not follow the conventional cross-section classification approach, instead the member capacity is determined based on the strain capacity of the elements that comprise the section. Element strain capacity is a continuous function of element local slenderness. (Gardner 2007). Although an elastic-perfectly-plastic material model is traditionally used to classify cross-section elements, more realistic material models including strain hardening are considered in CSM (Gardner et al. 2011).

For locally slender sections the concept of connecting cross-sectional slenderness to strain capacity has also been successfully implemented in the context of the inelastic bending reserve capacity of cold-formed steel members, and adopted in the Direct Strength Method (DSM) (Shiffaraw and Schafer 2012).

In this paper, a method complementary to CSM and DSM is proposed to calculate the strain capacity of cross-section elements based on local slenderness and connect the strain capacity to the rotation capacity of structural steel members. Accordingly, a continuous relationship between the rotation capacity of the members and the slenderness of the cross-sectional elements is achieved. To connect the element slenderness to strain capacity a comprehensive series of material and geometric shell finite element collapse analysis are performed in ABAQUS on component elements (plates) and the results are used to formulate the member rotation capacity. The results of I-shaped and box-shaped sections are compared to existing code provisions for both conventional and seismic design requirements and recommendations for potential improvements and future research are made.

2. Proposed Method

The proposed method to connect local slenderness to rotation capacity of the member has three main steps: (1) determine the element slenderness; (2) determine the strain capacity of the elements; (3) determine the member ductility based on the strain capacity. As shown in Fig.1, for box-shaped and I-shaped beams, the flange is assumed to be under uniform compression and it is also assumed that the member rotational ductility is controlled by the compression flange rather than instabilities in the web. These basic steps are elaborated in the following.

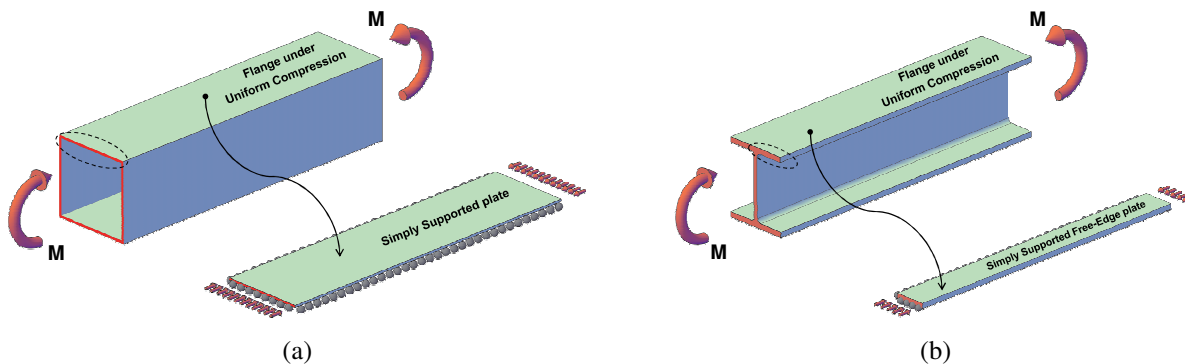


Figure 1: Structural members under bending moment (M): (a) Box-Shaped Section; (b) I-shaped Section.

2.1. Element slenderness

Element slenderness, λ_l , is a dimensionless parameter used to determine the elastic buckling load of plates, for a plate under longitudinal loading with yield stress, F_y and buckling stress F_{cr} :

$$\lambda_l = \sqrt{\frac{F_y}{F_{cr}}} = \frac{b}{t} \sqrt{\frac{F_y(12)(1-\nu^2)}{\pi^2 Ek}} \quad (1)$$

$$F_{cr} = \frac{F_y}{(\lambda_l)^2} \quad (2)$$

where b , is the width of the plate perpendicular to the direction of loading; t , is the thickness of the plate; E , is the Young's modulus; and ν , is the Poisson's ratio. The plate buckling coefficient, k , in Eq. 1 is a function of applied stress (i.e. uniform compression, bending, etc.), edge support conditions (i.e. free, simple, or clamped) and the plate length-to-width ratio. The plate buckling coefficient, k , is depicted in Fig.2 for a plate with different boundary conditions under uniform compression.

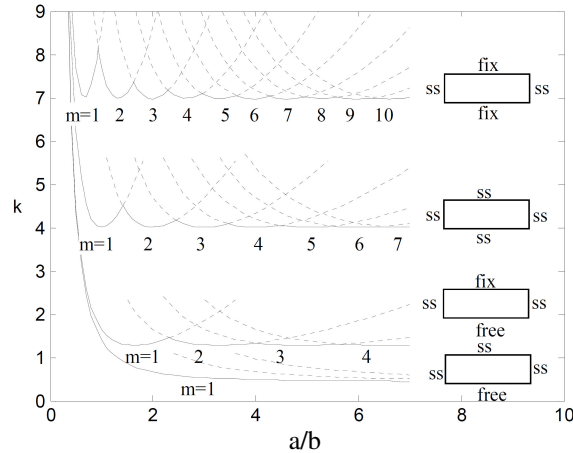
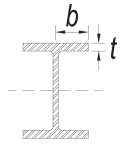
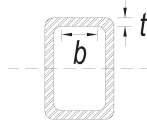


Figure 2: Plate buckling coefficient, k , as a function of normalized plate length (a/b) for different boundary conditions, m =number of buckled half-waves along the length of the plate. (ss: simply supported; fix: fixed supported or clamped; free: free edge or no support) (Yu and Schafer 2007)

For full members the boundary conditions along the edges of the elements that comprise the section are not ideal. Thus, in such cases the plate buckling coefficient, k , is also a function of the geometry of the attached elements. As an alternative, cross-section local buckling analysis may be used to determine F_{cr} directly, instead of using the isolated plate solutions. Shell finite element solutions or more efficient plate finite strip solutions may be utilized to efficiently find F_{cr} and hence λ_l for nearly any member. (see, e.g., Seif and Schafer 2010).

AISC traditionally has employed constant values for the plate buckling coefficient based on the element type (i.e. stiffened or unstiffened), stress type (axial or flexural compression) and cross-sectional shape (rolled or built-up I-shape, box-shape, HSS, etc.). Notably, these values are not explicitly provided in AISC specifications. However, Seif and Schafer (2010) back-calculated the assumed plate buckling coefficients utilized in the AISC Speciation, and these results are summarized in Table 1. The results of Table 1 are employed in Section 5 to compare the results developed herein to the code ductility limits.

Description ^{1,2,3}	Index ^{1,2}	Width-to-thickness ratio ^{1,2} b/t	Buckling coefficient ³ k	Limiting Slenderness λ_l^4	Example ¹
Flexure in flanges of rolled I-shaped sections and channels	λ_r	$1.0\sqrt{E/F_y}$	1.1	1.0	
	λ_p	$0.38\sqrt{E/F_y}$	1.1	0.38	
	λ_{md}	$0.38\sqrt{E/F_y}$	1.1	0.38	
	λ_{hd}	$0.30\sqrt{E/F_y}$	1.1	0.30	
Uniform compression in flanges of rolled I-shaped sections, plates projecting from rolled I-shaped sections; outstanding legs of pairs of angles in continuous contact and flanges of channels	λ_r	$0.56\sqrt{E/F_y}$	0.70	0.70	
	λ_p	-	-	-	
	λ_{md}	$0.38\sqrt{E/F_y}$	0.70	0.48	
	λ_{hd}	$0.30\sqrt{E/F_y}$	0.70	0.38	
Uniform compression in flanges of rectangular box and hollow structural sections of uniform thickness subject to bending or compression; flange cover plates and diaphragm plates between lines of fasteners or welds. (Applicable to columns in SMF systems and box sections used as beams or columns)	λ_r	$1.4\sqrt{E/F_y}$	4.43	0.70	
	λ_p	$1.12\sqrt{E/F_y}$	4.43	0.56	
	λ_{md}	$1.12\sqrt{E/F_y}$	4.43	0.56	
	λ_{hd}	$0.60\sqrt{E/F_y}$	4.43	0.30	

1. AISC-360-10 (AISC 2010a)
2. AISC-341-10 (AISC 2010b)
3. Seif and Schafer (2010)
4. ν is assumed to be 0.3 in calculating λ

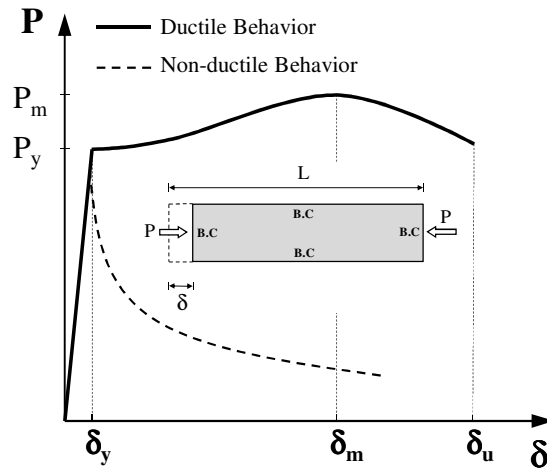


Figure 3: Plate behavior under applied load or displacement

2.2. Strain capacity of the elements

Strain capacity, ϵ_m , is the maximum compressive strain that can be applied to a ductile plate under compression before buckling. As shown in Fig. 3, the strain capacity of a ductile plate can be calculated by dividing the maximum plate displacement, δ_m (at peak load), by the length of the plate L as calculated in Eq. 3 and normalized to the yield strain, as shown in Eq. 4.

$$\varepsilon_m = \delta_m / L \quad (3)$$

$$\beta = \varepsilon_m / \varepsilon_y \quad (4)$$

where, β is the normalized strain capacity. It should be noted that the strain capacity could also be defined based on the ultimate displacement applied to the plate (δ_u). This approach would result in larger values for strain capacity. However, defining δ_u is complex for slender elements and potentially introduces other limit states (fracture). Accordingly, the strain capacity in this study may be conservative in some circumstances.

2.3. Member ductility based on the strain capacity

Connection of element strain capacity to member rotation capacity implies that each plane section along the length of the member remains perpendicular to the axial axis of the member, and each plane sections remains plane, i.e. Euler-Bernoulli beam theory. A detailed analytical formulation for connecting element strain capacity to the rotational ductility of flexural members is presented in Section 4. While the method is applicable to beam-columns, development of the method to beam-columns is under way.

3. Ductility of Cross-Section Elements

To determine the ductility of cross-section elements as a function of element slenderness, a comprehensive series of material and geometric shell finite element nonlinear collapse analyses were performed in ABAQUS (ABAQUS 2009) to obtain the nonlinear behavior of the plate under applied displacement and to calculate the strain capacity, according to the method discussed in Section 2.2.

3.1 Parametric numerical analyses

Parameters considered in the element deformation capacity study are are: (1) plate thickness, t ; (2) plate width, b ; (3) plate buckling coefficient, k ; and (4) yield stress, F_y . Each set of parametric analyses were performed based on specific ranges/assumptions for these parameters.

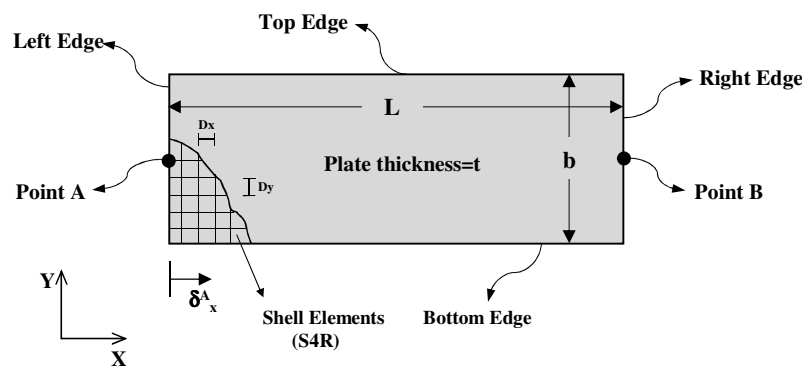


Figure 4: Parameters of the numerical model

As shown in Fig. 4, the studied plates were considered to be rectangular and were uniformly and finely meshed. As large strains were anticipated for stocky elements, a finite-strain shell element “S4R” suitable for large-strain analysis was selected. As shown in Table 2, four types of boundary conditions including both stiffened and unstiffened elements with simple and clamped boundary conditions were assumed. Moreover, three material types with different yield stress

were used to complete the parametric analysis. To study the sensitivity of the results to width of plate, the analyses were repeated for two other b values as described in Table 2. While the element slenderness (λ_l) was considered to be between 0.25 and 1.1, the plate thickness was calculated for each model in accordance with the formula in the last row of Table 2.

Table 2: Values of the parameters in the numerical models

Parameter	description	value
L	Plate length along x direction	250; 125, 250, 375 mm (for sensitivity analysis on b)
b	Plate length along y direction	50; 25, 50, 75 mm (for sensitivity analysis on b)
$D_x=D_y$	Element size in x, y directions	2.5; 1.25, 2.5, 3.75 mm (for sensitivity analysis on b)
λ_l	Slenderness	0.25~1.1
k	Plate buckling coefficient	Stiffened - Clamped Top and Bot. edge: $k=6.97$
		Stiffened - Simple Top and Bot. edge: $k=4.0$
		Unstiffened - Clamped Top edge and Free Bot. edge : $k=1.227$
		Unstiffened - Simple Top edge and Free Bot. edge : $k=0.425$
F_y	Yield stress	Material 1: $F_y = 235$ (N/mm ²)
		Material 2: $F_y = 275$ (N/mm ²)
		Material 3: $F_y = 355$ (N/mm ²)
t	Plate thickness	$t = \frac{b}{\lambda_l} \sqrt{F_y (12)(1-\nu^2) / (\pi^2 Ek)}$

For each type of plate, the assumed mathematical definition of all edge boundary conditions and constraints are provided in Table 3.

Table 3: Boundary conditions and constraints

Plate type	Top and Bottom B.C.	Mathematical Definition					
		Left edge	Point A ^{1,3}	Right edge	Point B ²	Top edge	Bottom edge
Stiffened	Clamped-Clamped	$u_z=0$	$u_y=0$	$u_x=u_z=0$	$u_y=0$	$u_z=0; \theta_x=0$	$u_z=0; \theta_x=0$
	Simple-Simple	$u_z=0$	$u_y=0$	$u_x=u_z=0$	$u_y=0$	$u_z=0$	$u_z=0$
Unstiffened	Clamped-Free	$u_z=0$	-	$u_x=u_z=0$	-	$u_y=u_z=0; \theta_x=0$	-
	Simple-Free	$u_z=0$	-	$u_x=u_z=0$	-	$u_y=u_z=0$	-

1. Left edge is constrained to Point A in x direction
2. Right edge is constrained to Point B in x direction
3. Displacement δ_x is applied to Point A

3.2 Geometric imperfections

To achieved realistic results, implementation of a proper geometric imperfection is necessary, especially in stocky regimes where the imperfection has an effect on both strength and strain capacity beyond the yield strain. The geometric imperfection is composed of an imperfection distribution and an imperfection amplitude/magnitude. If statistical data on actual imperfections is unavailable then more mathematical approaches are typically adopted.

Here the imperfection distribution is set to the 1st eigen-mode of the plate. The imperfection amplitude is commonly determined as a function of plate thickness (Zeinoddini and Schafer 2012). This method provides acceptable results in plates of small thicknesses and in cold-form steel design; but it can lead to unreasonably large imperfections in thicker plates. Several imperfection models have been proposed by Dawson and Walker (1972) which are amenable to estimating imperfection amplitude (ω_0) of plates, even in stocky regimes:

$$\text{Type-1: } \omega_0/t = \alpha \quad (5)$$

$$\text{Type-2: } \omega_0/t = \beta(\sigma_y/\sigma_{cr})^{0.5} \text{ or } \omega_0/t = \beta\lambda_l \quad (6)$$

$$\text{Type-3: } \omega_0/t = \gamma(\sigma_y/\sigma_{cr}) \text{ or } \omega_0/t = \gamma\lambda_l^2 \quad (7)$$

where, ω_0 is the imperfection amplitude, t is the plate thickness, and (α, β, γ) are real constants used to calibrate the various models. A summary of previous research on local geometric imperfections for stainless steel sections (Ashraf et. al. 2006b) demonstrates that Type 1, 2 or 3 imperfection models are the most common in the literature.

The expressions of Eq. (6) and (7) also may be written in an alternative form. Considering the definition of local slenderness:

$$\lambda_l = \frac{b}{t} \sqrt{\frac{F_y(12)(1-\nu^2)}{\pi^2 Ek}} = \frac{b}{t} C \quad (8)$$

$$C = \sqrt{\frac{F_y(12)(1-\nu^2)}{\pi^2 Ek}} \quad (9)$$

and then substituting into the preceding:

$$\text{Type-1: } \omega_0/t = \alpha \quad (10)$$

$$\text{Type-2: } \omega_0/t = \beta C \frac{b}{t} \Rightarrow \omega_0/b = \beta C \quad (11)$$

$$\text{Type-3: } \omega_0/t = \gamma \left(C \frac{b}{t}\right)^2 \Rightarrow \omega_0/t = \gamma C^2 \left(\frac{b}{t}\right)^2 \quad (12)$$

Thus, according to Eq. 10, ω_0/t in Type-1 has constant value for all values of the plate width, b . This model gives large imperfection values in stocky plates, which does not seem reasonable. Based on Eq. 11, ω_0 in Type-2 is actually a function of the plate width, b , and ω_0/b is constant for all values of the plate thicknesses. For Type-3, as per Eq. 12, ω_0/t is a function of both the plate thickness and the plate width. This model gives the most reasonable imperfection amplitude function, especially for low values of b/t , where smaller imperfections are expected. The comparison between the imperfection amplitude functions is schematically illustrated in Fig.5.

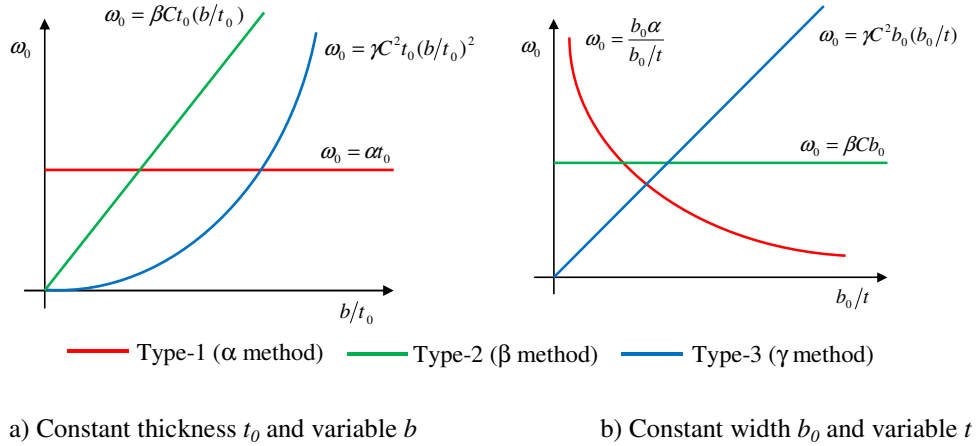


Figure 5: ω_0 vs b/t for all imperfection amplitude functions

Dawson and Walker (1972) indirectly calculated $\gamma=0.2$ by fitting a resistance function to available test results. However, more reasonable values for the imperfection coefficient have been presented for both structural steel and structural stainless steel by direct measurements. Gardner and Nethercot (2004b) recommend $\gamma=0.023$ for stainless steel tubes and Gardner et. al. (2010) proposed average value of $\gamma=0.066$ for both cold-formed and hot-rolled steel tubes. While structural steel members are considered in this study, the imperfection amplitude value was assumed to be calculated by Type-3 of imperfection function and $\gamma=0.066$. In the future, a statistical treatment of γ and comparison of the model error against available test data is needed.

3.3 Material models

To study the effect of the material model on the element strain capacity, three material models were considered: (1) elastic-perfectly-plastic; (2) bi-linear stain-hardening (Gardner et. al. 2011); and (3) multi-linear stain-hardening model (Galambos 2000), as shown in Fig. 6.

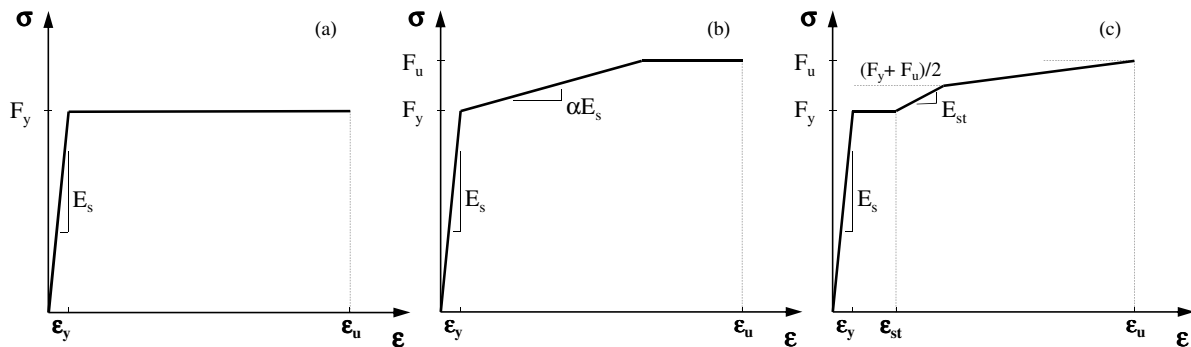


Figure 6: Material models: (a) elastic-perfectly-plastic model; (b) bi-linear stain-hardening model; (c) multi-linear stain-hardening model.

Where three material properties were considered in the parametric study, all required parameters are presented in Table 4. Material nonlinearities were accounted through classical metal plasticity theory based on von Mises yield criterion and isotropic hardening rule. The

engineering stress-strain values ($\sigma_{eng}, \epsilon_{eng}$) were converted to true stress-strain values ($\sigma_{True}, \epsilon_{True}$) by the following equation (ABAQUS 2009),

$$\epsilon_{True} = \ln(1 + \epsilon_{eng}) \quad (13)$$

$$\sigma_{True} = \sigma_{eng} (1 + \epsilon_{eng}) \quad (14)$$

Table 4: Material properties (Gioncu and Mazzolani 2002).

Material	F_y	F_u	ϵ_{st}	ϵ_u	E_s	E_{st}	ν	α
	N/mm ²	N/mm ²	mm/mm	mm/mm	N/mm ²	N/mm ²	-	-
Material-1	235	360	0.014	0.14	203000	5500	0.3	0.07
Material-2	275	430	0.015	0.12	203000	4800	0.3	0.07
Material-3	355	510	0.017	0.11	203000	4250	0.3	0.07

3.4 Results and formulation

The plate strain capacity was determined as a function of plate slenderness using the nonlinear shell finite element model and the results are provided in Fig. 7 for the three different material models. Each figure includes the results of 12 combinations of plate boundary conditions and material properties. As shown in the figures and summarized in Table 5, for the slenderness values larger than a specific limit, the plates did not show ductile behavior and buckling took place before yielding. However, for slenderness values less than this limit, ductile behavior was developed and can be assumed to be a function of plate slenderness. The plate strain capacity is connected to the plate slenderness by providing a quadratic exponential regression and the results are summarized in Table 5 for different material models. The results are compared to Gardner et al.'s (2011) relationship ($\epsilon_{csm}/\epsilon_y = 0.4/\lambda_p^{3.2}$) presented for strain capacity of steel members, where ϵ_{csm} is the CSM limiting strain (strain capacity in Continuous Strength Method) and λ_p is the plate slenderness. Although Gardner's relationship is valid only for $\epsilon_m/\epsilon_y \leq 15$, it is used here for larger values of ϵ_m/ϵ_y for comparison purposes.

Table 5: Strain Capacity

Material Model	Strain Capacity, $\beta = \epsilon_m/\epsilon_y$	Limit
elastic-Perfectly-Plastic	$e^{10.14\lambda_i^2 - 18.15\lambda_i + 7.8}$	$\lambda_i \geq 0.72$
bi-linear strain-hardening	$e^{9.48\lambda_i^2 - 17.81\lambda_i + 8.05}$	$\lambda_i \geq 0.76$
multi-linear strain-hardening	$e^{5.64\lambda_i^2 - 13.54\lambda_i + 7.12}$	$\lambda_i \geq 0.77$

To study the sensitivity of the results to the width of the plate a set of analyses was done for different values of the plate width as shown in Fig. 8. Accordingly, it is revealed that the results are not significantly related to the width of the plates, and λ_i is the key parameter.

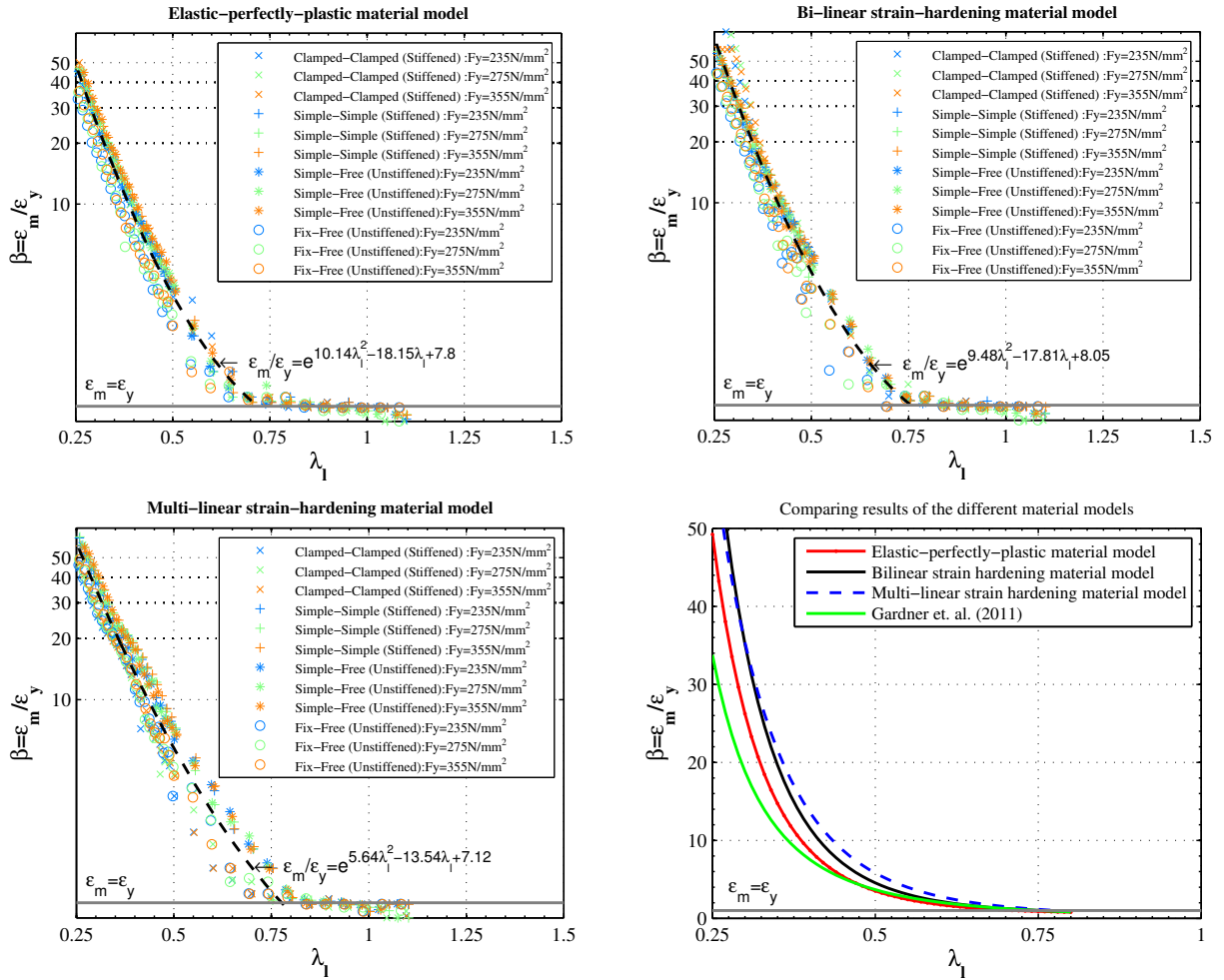


Figure 7: Element strain capacity for different material models

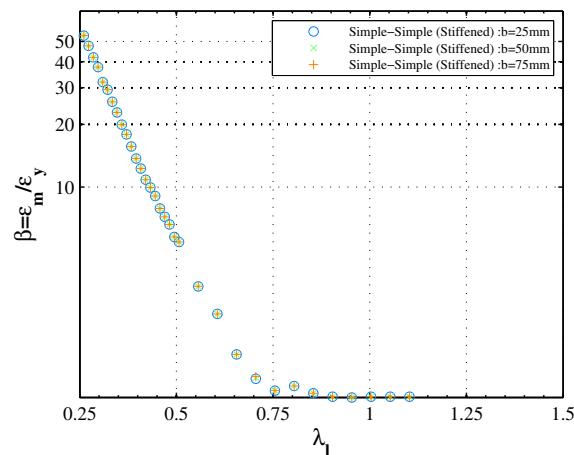


Figure 8: Sensitivity analysis on plate width, b

4. Member Ductility

Member ductility is the ability of member to undergo plastic deformation in terms of axial or rotational deformation without considerable degradation in the capacity. This study is primarily

focused on rotation capacity of structural steel members. Rotation capacity of the member has different definitions depending on its context and use for structural analysis or design. A common definition adopted in ASCE41-06 (ASCE 2007) and AISC documents (AISC 2010b) is to define the end rotation based on the chord rotation as shown in Fig. 9(a). The plastic hinge moment-rotation behavior is defined in Fig. 9(b) with more details, where M_y is the beam moment at first yielding, $M_p = ZF_y$ is the theoretical plastic moment, Z is the plastic modulus, M_m is the maximum mobilized moment (including strain hardening), θ_y is the beam plastic rotation at first yielding, θ_p is the beam elastic rotation at the level of plastic moment, θ_{pr} is the beam plastic rotation at the plastic moment, θ_m is the beam plastic rotation at M_m , and θ_u is the maximum beam rotation capacity including strength degradation to the level of the plastic moment.

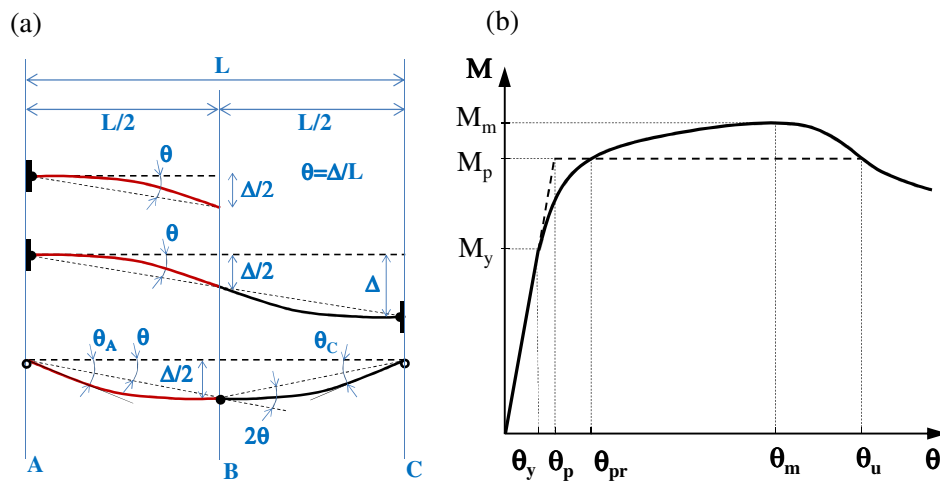


Figure 9: Definition of the beam rotation

It should be noted that other definitions also exist for plastic rotation based on the tangential rotations as discussed in Gardner et.al (2010). Accordingly, the plastic rotation of a simply supported beam at the midpoint is assumed to be the sum of the beam rotations at the beam ends ($\theta_A + \theta_C$). Although the results of this approach are almost similar to the chord-rotation method for large plastic rotations, the result of rotation at the plastic moment (θ_p) can be considerably different. It may be theoretically shown that θ_p calculated by the tangential definition is 1.5 times larger than θ_p obtained by the chord-rotation method. Therefore, these differences must be considered in comparison of the results of different studies.

4.1 Rotation at the plastic moment, θ_p

By assuming a linear moment distribution in the cantilever beam of Fig. 9(a), as shown in Fig. 10, and dividing the moment by EI (the flexural rigidity), the deflection of the beam can be calculated by implementing the Moment Area Theorem as following:

$$\Delta_B = \int_0^{L_{beam}} (L_{beam} - s) \frac{M(s)}{EI} ds = A_{M/EI} \bar{S}_B \quad (15)$$

where, Δ_B is the beam deflection at a point, $L_{beam} = L/2$ is the beam length, s is the distance from the point A, $M(s) = M_p(1 - s/L)$ is the beam moment distribution, $A_{M/EI}$ is the area under the curvature diagram and \bar{S}_B is the distance between point B and the centroid of $A_{M/EI}$. Accordingly, θ_p is calculated as following:

$$\theta_p = \frac{\Delta_B}{L_{beam}} = \frac{M_p L_{beam}}{3EI} = \frac{ZF_y L}{6EI} \quad (16)$$

By substituting $I = S \frac{d}{2}$ in Eq. 16, where S is the section modulus, and d is the beam depth, θ_p can be written as,

$$\theta_p = \frac{1}{3} \frac{Z}{S} \frac{L}{d} \frac{F_y}{E} = \frac{1}{3} S_F \frac{L}{d} \epsilon_y \quad (17)$$

According to the above equation, θ_p , is a function of length-to-depth ratio L/d , Shape factor, S_F , and yield strain, ϵ_y .

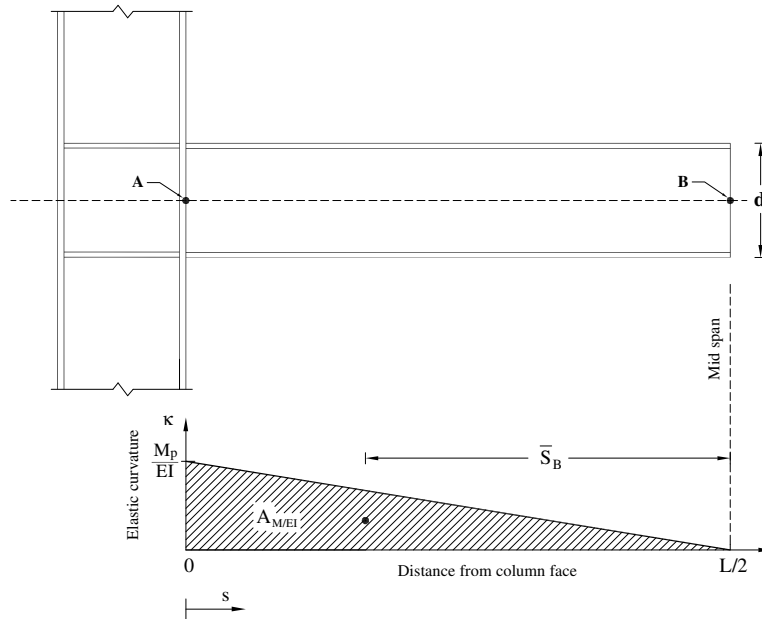


Figure 10: Calculating beam elastic rotation at the level of the plastic moment

4.2 Beam rotation at maximum moment, θ_m

Adopting Euler-Bernoulli bending and its basic kinematic assumptions, it is assumed that the axial bending strain varies linearly across the beam depth as following,

$$\epsilon = -\kappa y \quad (18)$$

where, ϵ is axial bending strain, $\kappa=1/\rho=d\theta/ds$ is the beam curvature, ρ is the radius of the bent beam, $d\theta$ is an infinitesimal angle of the element, ds is the length of the neutral axis along the element, and y is the distance to the neutral axis, as shown in Fig. 11.

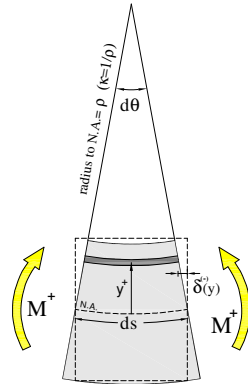


Figure 11: Bending deformation of an element

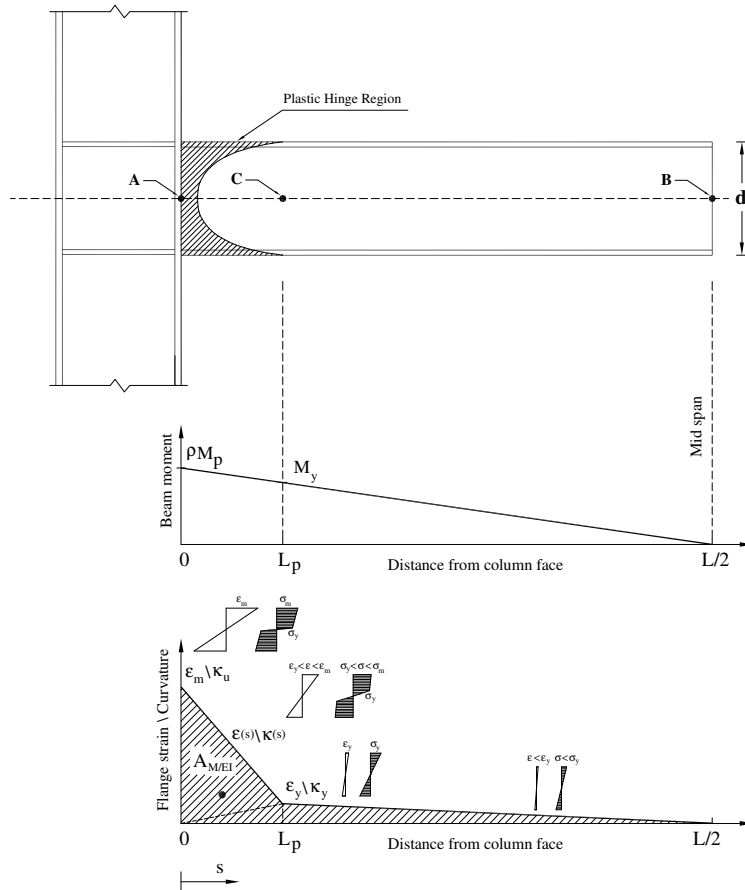


Figure 12: Beam bending moment distribution and flexural curvature along the length

Assuming a symmetric section of depth d , the beam curvature can be calculated based on the strain of the farthest fiber of the section,

$$\kappa = \frac{2\varepsilon}{d} \quad (19)$$

Therefore, the strain field of the section can be converted to the flexural curvature by considering the cross-section geometry. As discussed in Section 3, the strain capacity of the cross-sectional elements can be determined by knowing the element slenderness. Assuming a linear moment distribution, the maximum moment occurs at the end of the beam (Point A) where the maximum strain, ε_m , and bending curvature, κ_m , are anticipated. On the other hand, the flange strain equals to yield strain, ε_y , at the end of the plastic hinge region and beyond the plastic hinge region beam is considered to be elastic. By adopting a linear strain distribution within the plastic hinge region, the maximum strain of the beam is expressed in Eq. 18 and converted to beam curvature in Eq. 19. Both the strain and curvature distribution are also illustrated in Fig. 11.

$$\varepsilon(s) = \begin{cases} \varepsilon_m - \frac{\varepsilon_m - \varepsilon_y}{L_p} s & 0 \leq s \leq L_p \\ \varepsilon_y \left(1 - \frac{2s}{L}\right) & L_p \leq s \leq \frac{L}{2} \end{cases} \quad (20)$$

$$\kappa(s) = \begin{cases} \frac{2\beta\varepsilon_y}{d} - \frac{2(\beta-1)\varepsilon_y}{d.L_p} s & 0 \leq s \leq L_p \\ \frac{2\varepsilon_y}{d} \left(1 - \frac{2s}{L}\right) & L_p \leq s \leq \frac{L}{2} \end{cases} \quad (21)$$

where, L_p is the plastic hinge length and the other parameters are previously defined. To account for a more realistic material model, a bi-linear strain hardening model, see Fig.6 (b), is considered in the calculations. Due to strain-hardening, the maximum moment at the column face is considered to be ρM_p as shown in Fig.11 and the plastic hinge length can be calculated as following,

$$L_p = \frac{L}{2} \left(1 - \frac{M_y}{\rho M_p}\right) = \frac{L}{2} \left(1 - \frac{I}{\rho S_F}\right) \quad (22)$$

where, ρ is a coefficient for calculating the increase in plastic moment due to strain-hardening. By considering a bi-linear hardening behavior, the increase in plastic moment is calculated by Gardner et. al (2011) as following,

$$\rho = \frac{M_{csm}}{M_{pl}} = 1 + \frac{E_{sh}}{E} \frac{W_{el}}{W_{pl}} \left(\frac{\varepsilon_{csm}}{\varepsilon_y} - 1\right) - \left(1 - \frac{W_{el}}{W_{pl}}\right) \left(\frac{\varepsilon_{csm}}{\varepsilon_y}\right)^{-2} \quad (23)$$

where, M_{csm} is the maximum moment in the CSM method which corresponds to ρM_p herein, E_{sh}/E is the ratio of strain hardening modulus to Young's modulus that can be assumed to be

equal to α as shown in Fig. 6, $\varepsilon_{csm}/\varepsilon_y$ represents the strain capacity coefficient and is replaced by β , W_{pl}/W_{el} is the ratio of plastic modulus to elastic modulus and is equivalent to shape factor S_F . Correspondingly, Eq. 19 is summarized in a more compact form here as follows,

$$\rho = 1 + \frac{\alpha}{S_F}(\beta - 1) - \left(1 - \frac{1}{S_F}\right) \frac{1}{\beta^2} \quad (24)$$

Similar to the approach used to calculate the rotation at the plastic moment, θ_p , the beam rotation at maximum moment, θ_m , can be determined by dividing the beam tip displacement, calculated by the moment area method, by the beam length ($L/2$) as follows:

$$\theta_m = \left[\int_0^{L/2} \kappa(s) \left(\frac{L}{2} - s\right) ds \right] / (L/2) \quad (25)$$

where, $\kappa(s)$ is the flexural curvature as defined in Eq. 19. The integral in the numerator of Eq. 22 can be replaced by $A_M/EI \bar{S}_B$ as discussed in the previous section. Therefore, the beam rotation at the maximum moment, θ_m , can be derived as follows,

$$\theta_m = \frac{1}{6} \frac{L}{d} \varepsilon_y \left[\left(1 + \frac{1}{\rho S_F}\right) \left(1 - \frac{\beta}{\rho S_F}\right) + 2\beta \right] \quad (26)$$

According to Eq. 26, θ_m , is a function of length-to-depth ratio L/d , Shape factor S_F , strain capacity coefficient, β and yield strain, ε_y . Notably, as the strain capacity coefficient, β , is calculated based on the displacement at the maximum plate axial force (see Fig. 3), the obtained beam rotation is the rotation corresponding to the maximum mobilized moment. Further recall that β may be determined based on the plate element slenderness, λ_l .

In accordance with the definition of the rotation capacity in Appendix 1 of the AISC specification (AISC 2010a), rotation capacity, R , may be defined as follows,

$$R = \frac{\theta_m}{\theta_p} - 1 \quad (27)$$

Where, θ_m and θ_p are defined in Eq. 17 and Eq. 24, respectively. By substituting the values in Eq. 24 the rotation capacity is,

$$R = \frac{1}{2S_F} \left[\left(1 + \frac{1}{\rho S_F}\right) \left(1 - \frac{\beta}{\rho S_F}\right) + 2\beta \right] - 1 \quad (28)$$

As shown in Eq. 28 and Eq. 24, this definition of rotation capacity only depends on strain capacity coefficient, β , shape factor, S_F , and strain-hardening modulus coefficient α . Again, recall that $\beta = f(\lambda_l)$, e.g., per Table 5.

4.3 Sensitivity analysis on beam plastic rotation

To perform sensitivity analyses on these expressions, the shape factor of all W, M, S, HP and HSS sections section in the AISC manual are plotted versus the beam depth and a linear regression is established. Correspondingly, the shape factor is assumed to be 1.15 for I-shaped beams and 1.25 for box-shaped beams, as shown in Fig.13.

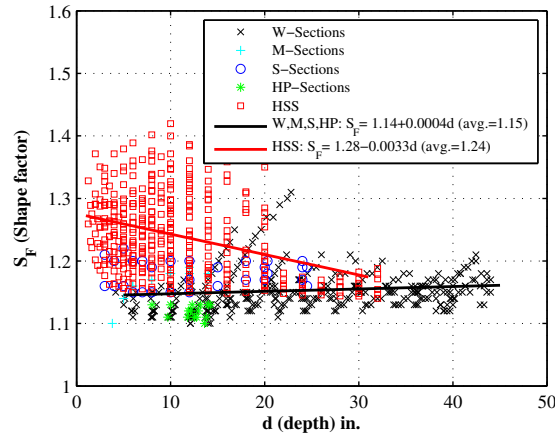


Figure 13: Shape factor of W, M, S, HP and HSS sections

The beam rotation at the maximum moment, versus the flange slenderness, for different values of Length-to-depth ratio (L/d) is provided in Fig. 14. According to Eq. 26, θ_m is linearly correlated to both L/d and ε_y , but λ_l is clearly the key variable.

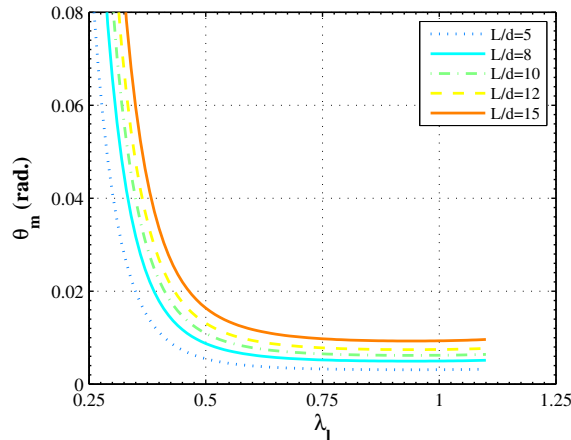


Figure 14: Sensitivity analysis on length-to depth ratio (L/d) of I-Shaped beams ($F_y = 355 \text{ N/mm}^2, S_F = 1.15$)

As shown in Fig. 15, the results of the sensitivity analysis on shape factor shows that both θ_m and R do not strongly depend on the shape factor for expected ranges. However, increases in the shape factor do result in increases in the rotation capacity as shown.

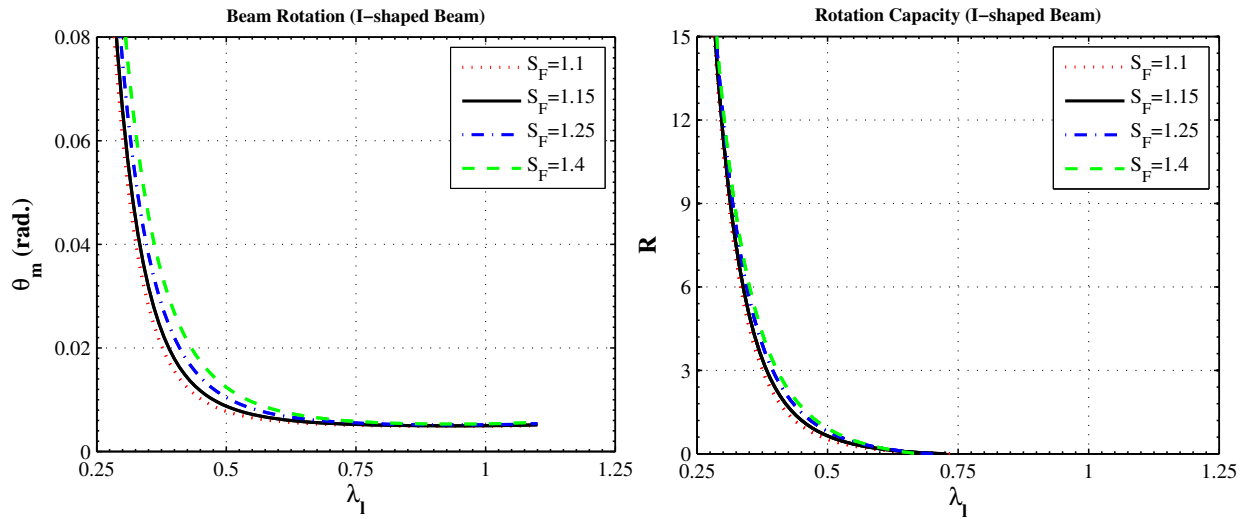


Figure 15: Sensitivity analysis on Shape factor, S_F . ($L/d = 8, F_y = 355 \text{ N/mm}^2$)

5. Comparison of the Results to Code Ductility Limits

The developed results are compared to the corresponding values in ASCE41-06, AISC-360-10 and AISC 341-10 for both compressive and flexural members in the following.

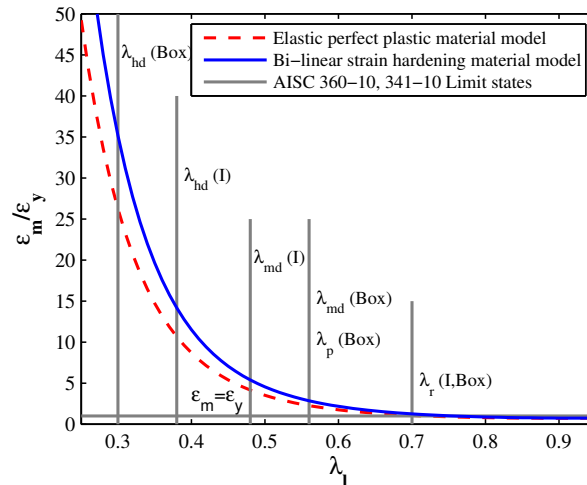


Figure 16: Axial strain capacity vs. slenderness

5.1 Compressive members

The axial strain capacity versus slenderness, and several code limits are depicted in Fig 16. The code limit values are as tabulated in Table 1. The horizontal line showing $\epsilon_m = \epsilon_y$ verifies that the λ_r limit in AISC clearly separates ductile and non-ductile elements. Based on the proposed method the compact limit λ_p corresponds to different levels of ductility in I-shaped and box-shaped sections and the I-shaped sections might have greater strain capacity for the same limit in AISC. Moreover, the elastic-perfectly-plastic material model provides more conservative results for axial ductility.

5.2 Flexural members

Both θ_m and R are compared to ASCE41-06, AISC-360-10 and AISC 341-10 in Fig. 17 for I-shaped beams and in Fig. 18 for box-shaped beams. As provided in the figures, the length-to-depth ratio is assumed to be 8 as a limit for no decrease in the plastic rotation capacity due to the length of the beam (ASCE 2007), F_y is considered to be 355 N/mm^2 (see material-3 in Table 4), and the shape factor is as discussed in Section 4.3.

The results show that the proposed method provides a continuous relationship between the element slenderness and the member rotation capacity, compared to the code results, which are typically use step-wise limits. As shown in Fig. 17, the results of the method developed here for I-shaped beams is in good agreement with the results of both AISC and ASCE41-06 for slenderness values less than 0.45; however, the result of ASCE41-06 for slenderness values more than 0.45 seems to be unconservative, while no ductility capacity is expected for slenderness values near and beyond 0.7. The developed method shows high ductility values for slenderness values less than 0.3. Limiting the ductility capacity to an upper limit, as done in the codes, is likely justified by the effects of lateral torsional buckling. Notably, the proposed method does not consider lateral torsional buckling in calculation of the beam rotation capacity.

Similar to the results for compression members, the ductility limit of compact members in box-shaped sections does not provide the expected ductility capacities, as shown in Fig. 18. Accordingly, it seems that the compact limits in box-members should be treated more cautiously. As discussed by Gardner et. al. (2011), even in test results, the rotational ductility of rectangular sections is not definite and it was shown that even for small values of slenderness relatively low ductility behavior may be observed.

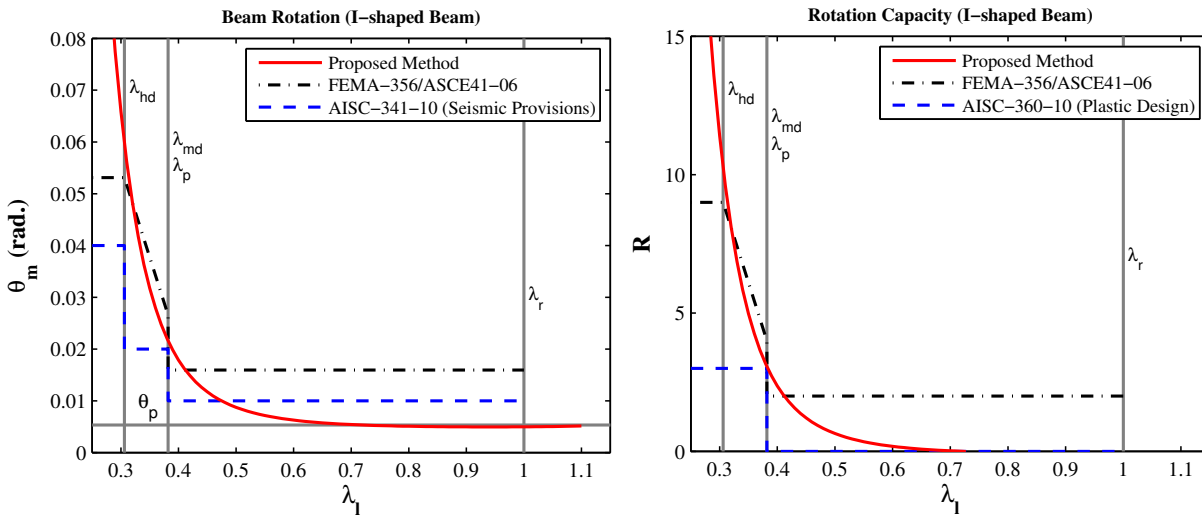


Figure 17: Comparison of θ_m and R of I-shaped beams to ASCE41-06 and AISC-360-10 and 341-10

$$(L/d = 8, F_y = 355 \text{ N/mm}^2, S_F = 1.15)$$

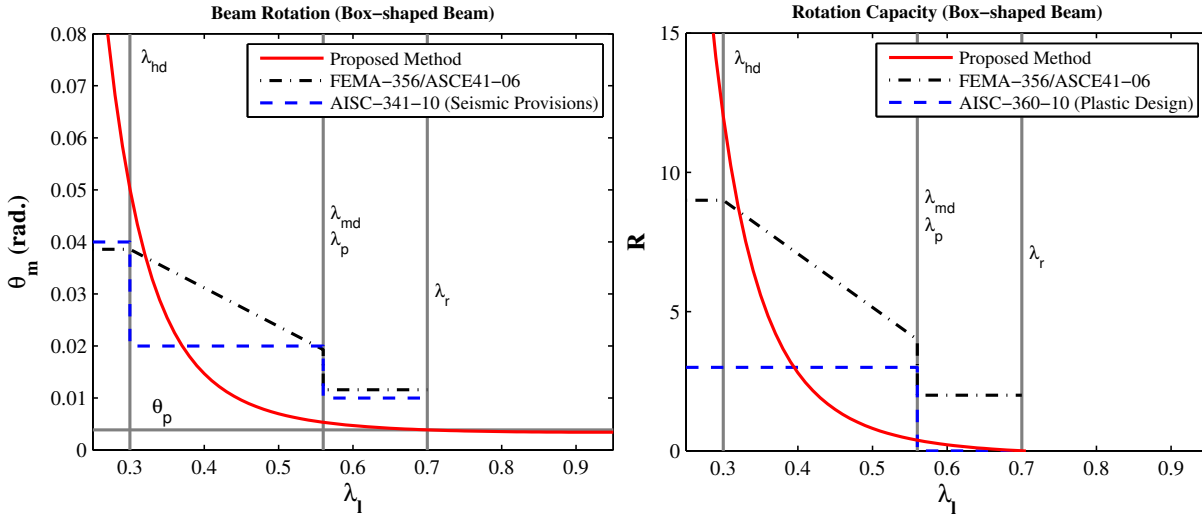


Figure 18: Comparison of θ_m and R of box-shaped beams to ASCE41-06 and AISC-360-10 and 341-10
 ($L/d = 8, F_y = 355 \text{ N/mm}^2, S_F = 1.25$)

6. Conclusions

Local plate slenderness has long been known to be the key parameter for predicting the load carrying capacity of slender plates. Herein it is shown the local plate slenderness is also the key parameter for determining the strain capacity of stocky plates. It is worth noting that essentially all plate conditions, including material properties, boundary conditions, and plate geometry are implicitly included in the plate slenderness. A solution is developed for determining the rotation capacity of a beam that utilizes this knowledge and predicts the maximum strain capacity of a beam to be a function of the flange local plate slenderness.

The derivation assumes Euler-Bernoulli beam theory, ignores lateral-torsional buckling, and presumes the flange (not the web) controls the section strain capacity. The role of beam length, beam depth, beam shape factor, and the beam material model in determining beam rotation capacity is also explicitly developed.

The developed method for determining the elastic and plastic curvature of a beam along its length is potentially beneficial for all existing methods for calculating the plastic rotation.

The calculated member rotation capacity of I-shaped beams is in good agreement with both AISC and ASCE41-06. However, AISC is a design code, and ASCE41-06 is focused more on analysis and sets forth parameters for modeling a plastic hinge as well as acceptance criteria for different performance levels. Accordingly, as expected AISC gives a lower bound result, and ASCE41 essentially an upper-bound result, as shown.

According to the results for box-section members, the compact limit of AISC might not provide the expected member behavior in plastic design. However, more studies including experimental investigations are needed to verify the method and to investigate the limits of the box-section members more precisely.

References

- ABAQUS. ABAQUS/Standard User's Manual, Version 6.9EF1. Pawtucket, RI; 2009.
- AISC/ANSI 360-10. (2010a). "Specification for structural steel buildings". Chicago (IL): *American Institute of Steel Construction, Inc.*
- AISC/ANSI 341-10. (2010b). "Seismic provisions for structural steel buildings". Chicago (IL): *American Institute of Steel Construction, Inc.*
- ASCE/SEI 41-06, ASCE standard. 2007. "Seismic Rehabilitation of Existing Buildings." *American Society of Civil Engineers*: New York, NY.
- Ashraf, M., Gardner, L., & Nethercot, D. A. (2006a). "Compression strength of stainless steel cross-sections". *Journal of Constructional Steel Research*, 62(1-2), 105–115.
- Ashraf, M., Gardner, L., & Nethercot, D. A. (2006b). "Finite element modelling of structural stainless steel cross-sections." *Thin-Walled Structures*, 44(10), 1048–1062.
- Ashraf, M., Gardner, L., & Nethercot, D. A. (2008). "Structural Stainless Steel Design: Resistance Based on Deformation Capacity". *Journal of Structural Engineering*, 134(3), 402–411.
- Dawson, R.G. , Walker A.C. (1972). "Post-buckling of geometrically imperfect plates." *Journal of the Structural Division, ASCE*, 98(1), 75–94.
- EN 1993-1-1. (2005). "Eurocode 3: Design of steel structures —Part 1-1: General Rules and Rules for Buildings", *European Standard, CEN*.
- FEMA-356. (2000). State of the art report on systems performance of steel moment frames subject to earthquake ground shaking. Federal Emergency Management Agency. Washington, DC; 2000.
- Galambos, T. V. (2000). "Recent research and design developments in steel and composite steel – concrete structures in USA." *Journal of Constructional Steel Research*, 55, 289-303.
- Gardner, L. (2008). "The continuous strength method". *Proceedings of the ICE - Structures and Buildings*, 161(3), 127–133.
- Gardner, L., Nethercot, D. A. (2004a). "Stainless steel structural design: a new approach". *The Structural Engineer*. 82(21), 21–28.
- Gardner, L., Nethercot, D. A. (2004b). "Numerical Modeling of Stainless Steel Structural Components — A Consistent Approach." *Journal of Structural Engineering*, 130(10), 1586–1601.
- Gardner, L., Saari, N., & Wang, F. (2010). "Comparative experimental study of hot-rolled and cold-formed rectangular hollow sections." *Thin-Walled Structures*, 48(7), 495–507.
- Gardner, L., Wang, F., & Liew, A. (2011). "Influence of Strain Hardening on the Behavior and Design of Steel Structures". *International Journal of Structural Stability and Dynamics*, 11(05), 855–875.
- Gioncu, V. , Mazzolani F.M. (2002). "Ductility of Seismic Resistant Steel Structures." 1st ed. London: *Spon Press-Taylor & Francis*.
- Seif, M., Schafer B.W. (2010). "Local buckling of structural steel shapes." *Journal of Constructional Steel Research*, 66, 1232-47.
- Shifferaw, Y., Schafer, B.W. (2012). "Inelastic Bending Capacity of Cold-Formed Steel Members." *Journal of Structural Engineering*, 138(4), 468–480.
- Yu, C., Schafer, B.W. (2007). "Effect of longitudinal stress gradients on elastic buckling of thin plates." *Journal of Engineering Mechanics*, 133(4), 452-463.
- Zeinoddini, V. M., Schafer, B.W. (2012). "Simulation of geometric imperfections in cold-formed steel members using spectral representation approach". *Thin-Walled Structures*, 60, 105–117.